7

Contrast Enhancement by Multiscale and Nonlinear Operators

Jian Fan and Andrew Laine

7.1 Introduction

Image enhancement techniques have been widely used in fields such as radiology, where the subjective quality of images is important for human interpretation (diagnosis). Contrast is an important factor in any subjective evaluation of image quality. Many algorithms for accomplishing contrast enhancement have been developed and applied to problems in medical imaging. A comprehensive survey of existing methods can be found in [1]. Among them, histogram modification and edge enhancement techniques have been most commonly used along with traditional methods of image processing.

Histogram modification techniques [2, 3] are attractive due to their simplicity and speed, and have achieved acceptable results for some applications. In general, a transformation function is derived from a desired histogram and the histogram of an input image. In general, the transformation function is almost always nonlinear. For continuous functions, a

lossless transformation may be achieved. However, for digital images with some finite number of gray levels, such a transformation results in information loss, due to quatization errors. For example, a subtle edge may be merged with its neighboring pixels and disappear. Attempts to incorporate local context into the transformation process have achieved limited success. For example, simple adaptive histogram equalization [4] supported by fixed contextual regions cannot adapt to features of distinct sizes.

Most edge enhancement algorithms share a common strategy implicitely: detection followed by local "edge sharpening". Unsharp masking is rare in that it has become a popular enhancement algorithm to assist radiologist in diagnosis [5, 6]. "Unsharp masking" sharpens edges by substracting a portion of a Laplacian fitered component from an original image. Theoretically, this technique was justified as an approximation of a deblurring process in [7]. Loo *et al.* [8] studied an extension of this technique in the context of radiographs. Another extension based on Laplacian fitering was proposed in [9]. However, these techniques of unsharp masking remain limited by their linear and single scale properties, and less effective for images containing a wide range of salient features typically found in digital mammography. In an attempt to overcome these limitations, a local contrast measure and nonlinear transform functions were introduced in [10], and subsequently refined in [11]. Unfortunately, limitations remained in these nonlinear methods as well: (1) They operated on a single scale, (2) No explicit noise suppression stage was included (in fact noise could be amplified), and (3) Ad-hoc nonlinear transform functions were introduced without a rigorous mathematical analysis of their enhancement mechanisms or the possible introduction of artifacts.

Recent advancement of wavelet theory has sparked researchers' interest in the application of image contrast enhancement [12, 13, 14, 15, 16, 17, 18]. These early studies showed promise, but were carried out at an experimental level. In this chapter, we give a detailed mathematical analysis of a dyadic wavelet transform, and reveal its connection to traditional techniques of unsharp masking. In addition, we propose a simple nonlinear enhancement function and analyze the problem of introducing artifacts, as a result of wavelet processing. Moreover, we describe an explict denoising stage that preserves edges using wavelet shrinkage [23] and adaptive thresholding.

These techniques are discussed in the following sections of this chapter:

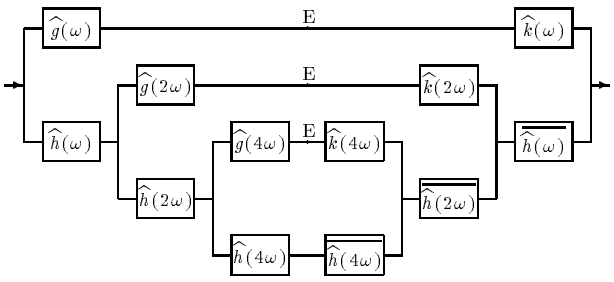

Figure 7.1: Computational structure for a one dimensional discrete dyadic wavelet transform (three levels shown).

Section 7.2 presents a one dimensional dyadic wavelet transform. Section 7.3 analyzes linear enhancement and its mathematical connection to traditional unsharp masking. Section 7.4 analyzes simple nonlinear enhancement by point-wise functional mapping. Section 7.5 introduces denoising with wavelet shrinkage along with an adaptive approach for finding threshold values. Section 7.6 presents a two-dimensional extension for digital mammography and special procedures developed for denoising and enhancement that avoid orientation distortions. Section 7.7 presents some sample experimental results and comparisons with existing techniques. Finally, Section 7.8 concludes our discussion and proposes possible future directions of research.

7.2 One-dimensional discrete dyadic wavelet transform

7.2.1 General structure and channel characteristics

A fast algorithm [20] for computing a 1-D redundant discrete dyadic wavelet transform (RDWT) is shown in Figure 7.1. The left side shows its decomposition structure, and the right, reconstruction. For an N-channel structure,

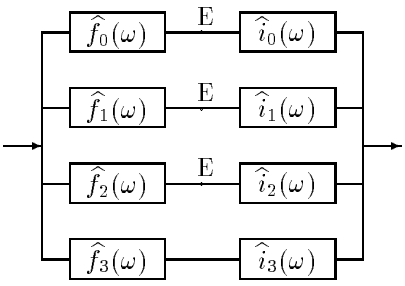

Figure 7.2: An equivalent multi-channel structure for a three-level RDWT.

there are $N-1$ high-pass or band-pass channels and a low-pass channel. Thus, the decomposition of a signal, produces $N-1$ sets of wavelet coefficients and a coarse signal.

Since there is no down-sampling and up-sampling shown in Figure 7.1, our redundant discrete dyadic wavelet transform does not correspond to an orthogonal wavelet basis (see Chapter 1, Section 1.3.2).

For simplicity of analysis, an equivalent multi-channel structure is shown in Figure 7.2. This computational structure also makes obvious the potential for high-speed execution by parallel processing.

We shall refer to filters $\widehat{f}_m(\omega)$ and $\widehat{i}_m(\omega)$ in Figure 7.2 as forward filters and inverse filters, respectively. Their relationship to filters $\widehat{g}(\omega)$, $\widehat{k}(\omega)$ and $\widehat{h}(\omega)$ are explicitly given by

$$\begin{aligned}
\widehat{f}_0(\omega) &= \widehat{g}(\omega), \quad \widehat{f}_N(\omega) = \prod_{l=0}^{N-1} \widehat{h}(2^l\omega), \\
\widehat{f}_m(\omega) &= \left[\prod_{l=0}^{m-1} \widehat{h}(2^l\omega)\right] \widehat{g}(2^m\omega), \ 1 \le m \le N-1.
\end{aligned}$$

and

$$\begin{aligned}
\widehat{i}_0(\omega) &= \widehat{k}(\omega), \quad \widehat{i}_N(\omega) = \prod_{l=0}^{N-1} \overline{\widehat{h}(2^l\omega)}, \\
\widehat{i}_m(\omega) &= \left[\prod_{l=0}^{m-1} \overline{\widehat{h}(2^l\omega)}\right] \widehat{k}(2^m\omega), \ 1 \le m \le N-1.
\end{aligned}$$

Since filters $\widehat{h}(\omega)$, $\widehat{g}(\omega)$ and $\widehat{k}(\omega)$ satisfy the condition

$$\left|\widehat{h}(\omega)\right|^2 + \widehat{g}(\omega)\widehat{k}(\omega) = 1, \tag{7.1}$$

filters $\widehat{f}_m(\omega)$ and $\widehat{i}_m(\omega)$ completely cover the frequency domain,

$$\sum_l \widehat{f}_l(\omega)\widehat{i}_l(\omega) = 1.$$

Channel frequency responses $\widehat{c}_m(\omega)$ can be written as

$$\widehat{c}_m(\omega) = \widehat{f}_m(\omega)\widehat{i}_m(\omega) = \begin{cases} 1 - \left|\widehat{h}(\omega)\right|^2, \ m = 0, \\ \prod_{l=0}^{m-1} \left|\widehat{h}(2^l\omega)\right|^2 \left[1 - \left|\widehat{h}(2^m\omega)\right|^2\right] \\ \qquad\qquad , \ 1 \le m \le (N-1), \\ \prod_{l=0}^{N-1} \left|\widehat{h}(2^l\omega)\right|^2, \ m = N. \end{cases}$$

As an example, we consider an extension of the class of filters proposed by Mallat *et al* in [20]

$$\widehat{h}(\omega) = e^{ip\frac{\omega}{2}} \left[\cos\left(\frac{\omega}{2}\right)\right]^{2n+p}, \tag{7.2}$$

where $p = 0$, or 1. Let

$$\widehat{\theta}_{m,q}(\omega) = \left[\prod_{l=0}^{m-1} \cos(2^{l-1}\omega)\right]^q,$$

then we can show that

$$\widehat{\theta}_{m,q}(\omega) = \left[\frac{\sin(2^{m-1}\omega)}{2^m \sin(\frac{\omega}{2})}\right]^q, \tag{7.3}$$

and therefore

$$\widehat{c}_m(\omega) = \begin{cases} \widehat{\theta}_{m,4n+2p}(\omega) - \widehat{\theta}_{m+1,4n+2p}(\omega) & , \ 0 \le m \le (N-1), \\ \widehat{\theta}_{N,4n+2p}(\omega) & , \ m = N. \end{cases} \tag{7.4}$$

Note that $\widehat{\theta}_{0,n}(\omega) = 1$, and for $0 < m < N$,

$$\begin{aligned} \widehat{c}_m(\omega) &= \widehat{\theta}_{m,4n+2p}(\omega) - \widehat{\theta}_{m+1,4n+2p}(\omega) \\ &= \sin^2\left(\frac{\omega}{2}\right) \ 4^m \widehat{\theta}_{m,4n+2p+2}(\omega) \sum_{l=0}^{2n+p-1} \left[\cos\left(2^{m-1}\omega\right)\right]^{2l}, \end{aligned} \tag{7.5}$$

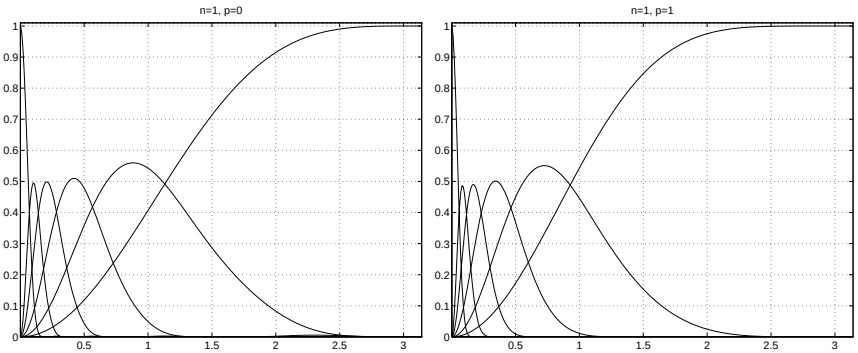

(a) (b)

Figure 7.3: Channel frequency responses for $N = 6, n = 1$ and (a) $p = 0$ and (b) $p = 1$.

and $\sin^2\left(\frac{\omega}{2}\right)$ is the frequency response of the discrete Laplacian operator of impulse response $\{1, -2, 1\}$.

$\widehat{\theta}_{m,q}(\omega)$ with even exponential q is an approximate Gaussian function, while the frequency responses of channels, $0 < m < N$, are approximately a Laplacian of Gaussian. Figure 7.3 shows each distinct channel frequency response, and Figure 7.4 compares $\widehat{\theta}_{2,4}(\omega)$ and $\widehat{\theta}_{2,6}(\omega)$ with related Gaussians.

7.2.2 Two possible filters

In this framework, the possible choices of filters are constrained by Equation (7.1). For the class of filters defined by Equation (7.2), we can derive

$$\widehat{g}(\omega)\widehat{k}(\omega) = \sin^2\left(\frac{\omega}{2}\right) \sum_{l=0}^{2n+p-1} \left[\cos\left(\frac{\omega}{2}\right)\right]^{2l}.$$

Under the constraint of both $\widehat{g}(\omega)$ and $\widehat{k}(\omega)$ being FIR's, there are two possible choices distinguished by the order of zero's in their frequency responses.

1. **Laplacian filter**. In this case, $\widehat{g}(\omega) = -4\left[\sin\left(\frac{\omega}{2}\right)\right]^2$ or $g(l) = \{1, -2, 1\}$, which defines a discrete Laplacian operator, such that $(g * s)(l) = s(l+1) - 2s(l) + s(l-1)$. Accordingly, we can chose both

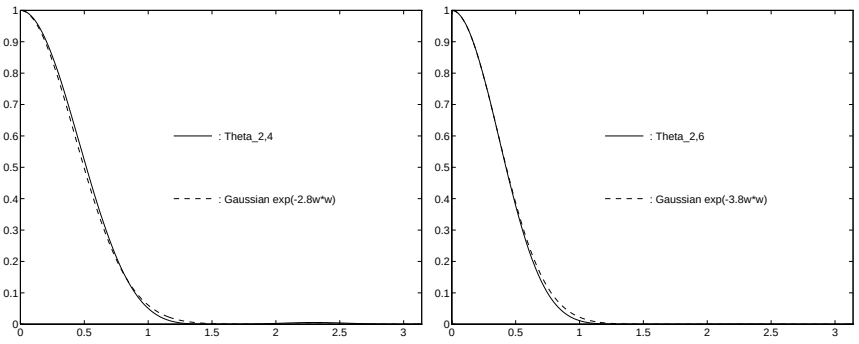

(a) (b)

Figure 7.4: (a) $\widehat{\theta}_{2,4}(\omega)$ compared with the Gaussian function $e^{-2.8\omega^2}$.
(b) $\widehat{\theta}_{2,6}(\omega)$ compared with the Gaussian function $e^{-3.8\omega^2}$.

filters $\widehat{h}(\omega)$ and $\widehat{k}(\omega)$ to be symmetric,

$$\widehat{h}(\omega) = \left[\cos\left(\frac{\omega}{2}\right)\right]^{2n}$$

and

$$\widehat{k}(\omega) = \frac{1 - \left|\widehat{h}(\omega)\right|^2}{\widehat{g}(\omega)} = -\frac{1}{4}\sum_{l=0}^{2n-1}\left[\cos\left(\frac{\omega}{2}\right)\right]^{2l}.$$

Both forward and inverse filters, $0 \le m \le N-1$, can be derived by

$$\begin{aligned}\widehat{f}_m(\omega) &= -4\left[\sin(2^{m-1}\omega)\right]^2\widehat{\theta}_{m,2n}(\omega) \\ &= -4\sin^2\left(\frac{\omega}{2}\right)4^m\widehat{\theta}_{m,2n+2}(\omega) = \widehat{g}(\omega)\widehat{\lambda}_m(\omega)\end{aligned} \tag{7.6}$$

and

$$\widehat{i}_m(\omega) = -\widehat{\theta}_{m,2n}(\omega)\frac{1}{4}\sum_{l=0}^{2n-1}\left[\cos\left(2^{m-1}\omega\right)\right]^{2l} = -\widehat{\gamma}_m(\omega).$$

Note that the forward filters $\widehat{f}_m(\omega)$, $0 < m < N$, can be interpreted as two cascaded operations, a Gaussian averaging of $\widehat{\theta}_{m,2n+2}(\omega)$ and the Laplacian $-4\left[\sin(\frac{\omega}{2})\right]^2$, while the set of inverse filters $\widehat{i}_m(\omega)$ are low-pass filters. For an input signal $s(l)$, wavelet coefficients at the points "E" (as shown in Figures 7.1 and 7.2) may be written as

$$w_m(l) = \Delta(s * \lambda_m)(l)$$

where Δ is the discrete Laplacian operator, and $\lambda_m(l)$ is approximately a Gaussian filter. This means that each wavelet coefficient $w_m(l)$ is dependent on the local contrast of the original signal at each position l.

2. **Gradient filter**. In this case, $\widehat{g}(\omega) = 2ie^{-i\frac{\omega}{2}}\sin\left(\frac{\omega}{2}\right)$, or $g(0) = 1$, and $g(1) = -1$, such that $(g * s)(l) = s(l) - s(l-1)$. Thus we select the filters

$$\widehat{h}(\omega) = e^{i\frac{\omega}{2}}\left[\cos\left(\frac{\omega}{2}\right)\right]^{2n+1}$$

and

$$\widehat{k}(\omega) = -e^{i\omega}\widehat{g}(\omega)\ \frac{1}{4}\sum_{l=0}^{2n}\left[\cos\left(\frac{\omega}{2}\right)\right]^{2l}.$$

We then derived the forward filters

$$\widehat{f}_m(\omega) = \widehat{g}(\omega)2^m\widehat{\theta}_{m,2n+2}(\omega) = \widehat{g}(\omega)\widehat{\lambda}_m(\omega)$$

and inverse filters

$$\widehat{i}_m(\omega) = -e^{i\omega}\widehat{g}(\omega)\widehat{\gamma}_m(\omega),$$

where

$$\widehat{\gamma}_m(\omega) = 2^m\widehat{\theta}_{m,2n+2}(\omega)\frac{1}{4}\sum_{l=0}^{2n}\left[\cos\left(2^{m-1}\omega\right)\right]^{2l}$$

is a low-pass filter.

In this case, the associated wavelet coefficients may be written as

$$w_m(l) = \nabla(s * \lambda_m)(l)$$

where ∇ is a discrete gradient operator characterized by $\nabla s(l) = s(l) - s(l-1)$.

7.3 Linear enhancement and unsharp masking

7.3.1 Review of unsharp masking

An early prototype of unsharp masking [7] was

$$s_u(x,y) = s(x,y) - k\Delta s(x,y), \tag{7.7}$$

where $\Delta = \frac{\partial^2}{\partial x^2} + \frac{\partial^2}{\partial y^2}$ is the Laplacian operator. However, this original formula worked only at the level of finest resolution. More versatile formulas were later developed in two distinct ways.

One way to extend this original formula was based on exploiting the averaging concept behind the Laplacian operator. The discrete form of the Laplacian operator may be written as

$$\begin{aligned}\Delta s(i,j) &= [s(i+1,j) - 2s(i,j) + s(i-1,j)] + [s(i,j+1) - 2s(i,j) + s(i,j-1)] \\ &= -5\left\{ s(i,j) - \frac{1}{5}\left[s(i+1,j) + s(i-1,j) + s(i,j) + s(i,j+1) + s(i,j-1)\right]\right\}\end{aligned}$$

This formula shows that the discrete Laplacian operator can be implemented by substracting from the value of a central point its average neighborhood. Thus, an extended formula [8] can be written as

$$s_u(i,j) = s(i,j) + k\left[s(i,j) - (s * h)(i,j)\right], \tag{7.8}$$

where $h(i,j)$ is a discrete averaging filter, and $*$ denotes convolution. In [8], an equal-weighted averaging mask was used:

$$h(x,y) = \begin{cases} 1/N^2, & |x| < N/2, |y| < N/2 \\ 0, & \text{otherwise.} \end{cases}$$

Another way to extend the prototype formula [9] came from the idea of a Laplacian-of-Gaussian filter, which expands Equation (7.7) into

$$s_u(x,y) = s(x,y) - k\Delta(s * g)(x,y) = s(x,y) - k(s * \Delta g)(x,y), \tag{7.9}$$

where $g(x,y)$ is an Gaussian function, and $\Delta g(x,y)$ is a Laplacian-of-Gaussian filter.

We mention for future reference, that both extensions shown in Equations (7.8) and (7.9) are limited to a single scale.

7.3.2 Inclusion of unsharp masking within RDWT framework

Next, we shall prove that unsharp masking with a Gaussian lowpass filter is included in a dyadic wavelet framework for enhancement by considering two special cases of linear enhancement .

In the first case, transform coefficients of channels $0 \leq m \leq N-1$ are enhanced (multiplied) by the same gain $G_0 > 1$, or $G_m = G_0 > 1$, $0 \leq m \leq N-1$. The system frequency response is thus

$$\begin{aligned} \widehat{v}(\omega) &= \sum_{m=0}^{N-1} G_m \widehat{c}_m(\omega) + \widehat{c}_N(\omega) = G_0 \sum_{m=0}^{N} \widehat{c}_m(\omega) - (G_0 - 1)\widehat{c}_N(\omega) \\ &= G_0 - (G_0 - 1)\widehat{c}_N(\omega) = 1 + (G_0 - 1)\left[1 - \widehat{c}_N(\omega)\right]. \end{aligned}$$

This makes the input-output relationship of the system simply

$$s_e(l) = s(l) + (G_0 - 1)\left[s(l) - (s * c_N)(l)\right]. \tag{7.10}$$

Since $\widehat{c}_N(\omega)$ is approximately a Gaussian lowpass filter, Equation (7.10) may be seen as the 1-D counterpart of Equation (7.8).

In the second case, transform coefficients of a single channel p, $0 \leq p < N$ are enhanced by a gain $G_p > 1$, thus

$$\begin{aligned} \widehat{v}(\omega) &= \sum_{m \neq p} \widehat{c}_m(\omega) + G_p \widehat{c}_p(\omega) \qquad (7.11) \\ &= \sum_{m=0}^{N} \widehat{c}_m(\omega) + (G_p - 1)\widehat{c}_p(\omega) = 1 + (G_p - 1)\widehat{c}_p(\omega). \end{aligned}$$

Recall channel frequency response $\widehat{c}_m(\omega)$ derived previously in 7.5, the input-output relationship of the system (7.11) can be written as

$$s_e(l) = s(l) - (G_p - 1) \cdot \Delta(s * \eta)(l), \tag{7.12}$$

where $\eta(l)$ is the impulse response of an approximate Gaussian filter. Similarily, Equation (7.12) may be seen as the 1-D counterpart of Equation (7.9).

The inclusion of these two forms of unsharp masking demonstrates the flexibility and versatility of a dyadic wavelet framework.

7.4 Nonlinear enhancement by functional mapping

Linear enhancement can be seen as a mapping of wavelet coefficients by a linear function $E_m(x) = G_m x$. Therefore, a direct extension of this is a nonlinear mapping function $E_m(x)$. The main challenges here are how to design a nonlinear function and how to best utilize multichannel information extracted from a dyadic wavelet framework to accomplish contrast enhancement.

7.4.1 Minimum constraint for an enhancement function

A major concern for our enhancement scheme was to introduce no artifacts during processing and reconstruction. For the dyadic wavelet framework adopted, this meant that we could not create new extrema in the channel outputs. This defined a minimum constraint on any enhancement function, that is, such a function must be continuous and monotonically increasing.

7.4.2 Filter selection

For linear enhancement, selection of filters $\widehat{g}(\omega)$ (and thus $\widehat{k}(\omega)$) made no difference. However, this was not true for the nonlinear case. For this particular nonlinear approach, our analysis showed that a Laplacian filter should be favored.

By selecting a Laplacian filter, we can be assured that positions of extrema will be unchanged and that no new extrema will be created within each channel. This is possible because:

1. Laplacian filters are zero-phase. No spatial shifting exists in the transform space.

2. A monotonically increasing function $E(x)$ will not produce new extrema. (At some point x_0, $E\left[f(x_0)\right]$ is an extrema if and only if $f(x_0)$ was an extrema).

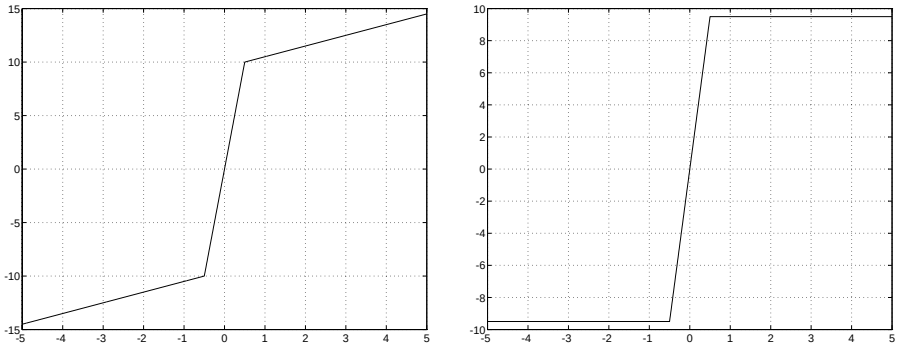

(a) (b)

Figure 7.5: (a) $E(x)$ and (b) $\delta(x)$, both with $T = 0.5$ and $K = 20$.

3. The reconstruction filters are simply zero-phase smoothing filters which will not create extrema.

The major difficulty for using a gradient filter is that reconstruction includes another gradient operator. As a result, a monotonically increasing function $E(x)$ alone will no longer guarantee new extrema will not be introduced in each *output channel*. Moreover, it is not difficult to show that any nonlinear mapping will change the positions of original extrema. Therefore, we shall assume the choice of Laplacian filters in the remainder of this section.

7.4.3 A nonlinear enhancement function

Designing a nonlinear enhancement scheme is made difficult due to two reasons: (1) the problem of defining a criteria of optimality for contrast enhancement. (2) complexity of analyzing nonlinear systems. We adopted the following guidelines in designing our nonlinear enhancement functions:

(1) An area of low contrast should be enhanced more than an area of high contrast. This is equivalent to saying that small values of $w_m[l]$ should have larger gains.

(2) A sharp edge should not be blurred.

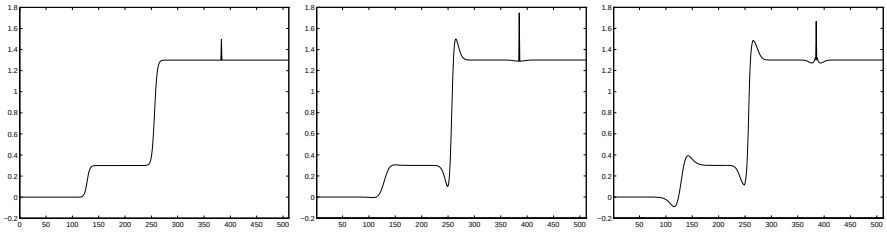

(a) (b) (c)

Figure 7.6: 1-D contrast enhancement of a synthetic signal (a) by four-level dyadic wavelet analysis with (b) a linear operator with $K_0 = 2.3$, and (c) a nonlinear operator with $t = 0.1$ and $K_0 = 7$.

Experimentally, we found the following simple function advantageous:

$$E(x) = \left\{ \begin{array}{ll} x - (K-1)T & , \text{ if } x < -T \\ Kx & , \text{ if } |x| \leq T \\ x + (K-1)T & , \text{ if } x > T \end{array} \right\} = x + \delta(x) \qquad (7.13)$$

where $K > 1$ and

$$\delta(x) = \left\{ \begin{array}{ll} -(K-1)T, & \text{if } x < -T, \\ (K-1)x, & \text{if } |x| \leq T, \\ (K-1)T, & \text{if } x > T. \end{array} \right.$$

The enhancement operator δ_m has two free parameters: threshold T_m and gain K_m. In our experimental studies, $K_m = K_0$, $0 \leq m \leq N-1$, and $T_m = t \times \max\{|w_m[n]|\}$, where $0 < t \leq 1$ was user specified. For $t = 1.0$, wavelet coefficients at levels $0 \leq m \leq N-1$ were multiplied by a gain of K_0, shown previously to be mathematically equivalent to unsharp masking . Thus our nonlinear algorithm includes unsharp masking as a subset. Figure 7.6 shows a numerical example, comparing linear and nonlinear enhancement. Note the lack of enhancement for the leftmost edge, in the case of the linear operator.

Specifically, an enhanced signal $s_e(l)$ can be written as

$$\begin{aligned} s_e(l) &= \sum_{m=0}^{N-1} (E_m \left[(s * f_m)\right] * i_m)(l) + (s * f_N * i_N)(l) \\ &= \sum_{m=0}^{N} (s * f_m * i_m)(l) + \sum_{m=0}^{N-1} (\delta_m \left[\Delta(s * \lambda_m)\right] * i_m)(l) \end{aligned}$$

or,

$$s_e(l) = s(l) - \sum_{m=0}^{N-1} (\delta_m \, [\Delta(s * \lambda_m)] * \gamma_m)(l). \tag{7.14}$$

For completeness, we mention that the formula of Equation (7.14) can be seen as a multiscale and nonlinear extension of the original unsharp masking defined by Equation (7.9). We argue that multiscale unsharp masking as defined by Equation (7.14) makes a marked improvement over traditional techniques in two respects:

1. The fast multiscale (or multimask) decomposition efficiently identifies features existing within distinct levels of scale, eliminating the need for search.

2. The nonlinear algorithm enhances small features within each scale without blurring the edges of larger features, making possible the simultaneous enhancement of features of all sizes.

7.5 A methodology for combined denoising and enhancement

The nonlinear enhancement methods proposed previously [11] did not take into account the presence of noise. In general, noise exists in a digitized image, due to the imaging device (acquisition) and quantization. As a result of nonlinear processing, noise may be amplified and may diminish any benefit of enhancement.

Unfortunately, denoising a radiograph (or any medical image) is a very difficult problem for two reasons. Fundamentally, there is no absolute boundary to distinguish a feature from noise. Even if there are known characteristics of a certain type of noise, it may be theoretically impossible to completely seperate the noise from features of interest. Therefore, most denoising methods may be seen as ways to suppress very high frequency and incoherent components of an input signal.

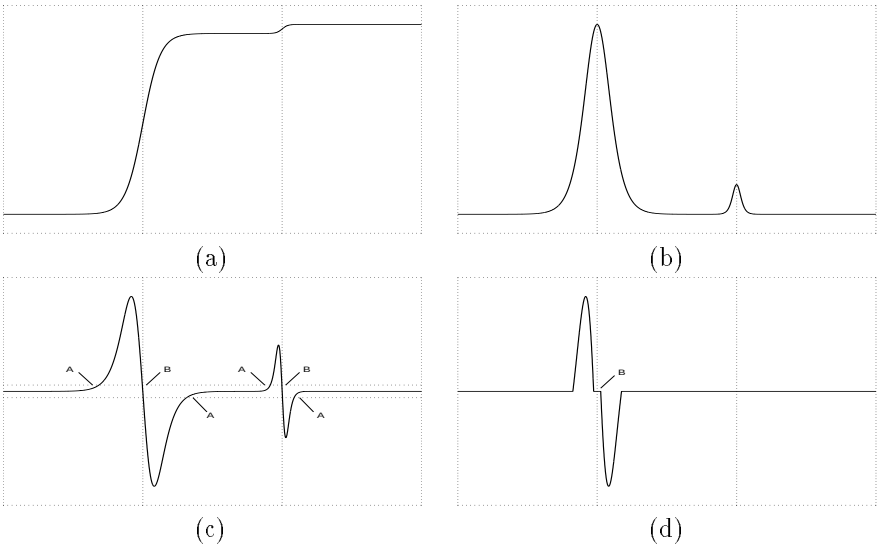

Figure 7.7: (a) Signal with two edges. (b) 1st derivative (gradient). (c) 2nd derivative (Laplacian). (d) Shrunken 2nd derivative.

A naive method of denoising that is equivalent to low-pass filtering is naturally included in any dyadic wavelet framework. That is, simply discard several channels of highest resolution, and enhance channels confined to lower frequency. The problem associated with this linear denoising approach is that edges are blurred significantly. This flaw makes linear denoising unsuitable within a contrast enhancement scheme targeted for medical imaging. Figure 7.9 (c) shows an example of this approach. In order to achieve edge-preserved denoising, more sophisticated methods based on wavelet analysis were proposed in the literature. Mallat and Hwang [22] connected noise behavior to singularities. Their algorithm relied on a multiscale edge representation. The algorithm traced modulus wavelet maxima to evaluate local Lipschitz exponents and deleted maxima points with negative Lipschitz exponents. Donoho [23] proposed nonlinear wavelet shrinkage. This algorithm reduced wavelet coefficients towards zero based on a level-dependent threshold.

7.5.1 incorporating wavelet shrinkage into enhancement

The method of wavelet shrinkage can be incorporated trivially into our nonlinear enhancement framework by simply adding an extra segment to the enhancement function $E(x)$, defined earlier in Equation (7.13).

$$E(x) = \begin{cases} x - (K-1)T_e + KT_n & , \text{ if } x \leq -T_e \\ K(x + T_n) & , \text{ if } -T_e \leq x \leq -T_n \\ 0 & , \text{ if } |x| \leq T_n \\ K(x - T_n) & , \text{ if } T_n \leq x \leq T_e \\ x + (K-1)T_e - KT_n & , \text{ if } x \geq T_e \end{cases} \tag{7.15}$$

However, there are two arguments which favor shrinking *gradient coefficients* instead of *Laplacian coefficients*.

First, gradient coefficients exhibit a higher signal to noise ratio (SNR). For any shrinkage scheme to be effective, an essential property is that the magnitude of a signal's components be larger than that of existing noise (at least most of the time). It is thus sensible to define the SNR as the maximum magnitude of a signal over the maximum magnitude of noise. For example, consider a soft edge model $f(x) = A/(1 + e^{-2\beta x}),\ A > 0$. Its first and second derivatives are $f'(x) = A\beta/\left[2\cosh^2(\beta x)\right]$ and $f''(x) = -A\beta^2 \sinh(\beta x)/\cosh^3(\beta x)$, with magnitude of local extrema $|f'(x_0)| = A|\beta|/3$ and $|f''(x_0)| = 2A\beta^2/3\sqrt{3}$, respectively. In this simple model, we can assume that noise is characterized by a relatively small A value and large β value. Clearly, gradient coeffcients have a higher SNR than that of Laplacian coefficients since β contributes less. Figures 7.7 (b) and (c) show first and second derivatives, respectively, for an input signal (a) with two distinct edges.

In addition, boundary contrast is not affected by shrinking gradient coefficients. As shown in Figure 7.7, coefficients aligned to the boundary of an edge are local extrema in the case of a first derivative (gradient), and zero crossings in the case of a second derivative (Laplacian). For a simple point-wise shrinking operator, there is no way to distinguish the points marked "B" from the points marked "A". As a result, regions around each "A" and "B" point are diminished, while the discontinuity in "B" (Fig. 7.7) sacrifices boundary contrast.

In the previous section, we argued that nonlinear enhancement is best

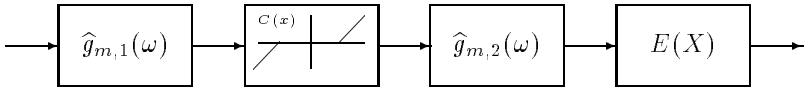

Figure 7.8: Incorporating wavelet shrinkage into an enhancement framework (one level shown).

performed on Laplacian coefficients. Therefore, in order to incorporate denoising into our enhancement algorithm, we split the Laplacian operator into two cascaded gradient operators. Note that

$$\widehat{g}_m(\omega) = -4\left[\sin\left(2^{m-1}\omega\right)\right]^2 = \widehat{g}_{m,1}(\omega)\widehat{g}_{m,2}(\omega)$$

where

$$\begin{cases} \widehat{g}_{m,1}(\omega) = e^{-i\omega/2}2i\sin\left(\frac{\omega}{2}\right), \widehat{g}_{m,2}(\omega) = e^{i\omega/2}2i\sin\left(\frac{\omega}{2}\right) & , \text{ if } m = 0, \\ \widehat{g}_{m,1}(\omega) = \widehat{g}_{m,2}(\omega) = 2i\sin\left(2^{m-1}\omega\right) & , \text{ otherwise.} \end{cases}$$

Denoising by wavelet shrinkage [23] can then be incorporated into this computational structure as illustrated in Figure 7.8, where the shrinking operator can be written as

$$C(x) = sign(x) \cdot \begin{cases} |x| - T_n & , \text{if } |x| > T_n, \\ 0 & , \text{ otherwise.} \end{cases}$$

Note that the shrinking operator is a piece-wise linear and monotonically non-decreasing function. Thus in practice, the shrinking operator will not introduce artifacts.

7.5.2 Threshold estimation for denoising

The threshold T_n is a critical parameter in the shrinking operation. For a white noise model and orthogonal wavelet, Donoho [23] suggested a formula of $T_n = \sqrt{2\log(N)}\sigma/\sqrt{N}$, where N is the length of a input signal and σ is the standard deviation of wavelet coefficients. However, the dyadic wavelet we applied is not an orthogonal wavelet. Moreover, in our 2-D applications, a shrinking operation is applied to magnitudes of gradient coefficients instead of wavelet coefficients themselves. Therefore, a method of threshold estimation method proposed in [24] for edge detection may be more suitable.

In our "shrinking" operation, only the magnitudes of the gradient of a Gaussian low-passed signal are modified. As pointed out in [24], for white Gaussian noise, the probability distribution function of the magnitudes of gradient is characterized by the Rayleigh distribution:

$$Pr_{\|\Delta f\|}(m) = \begin{cases} \frac{m}{\eta^2} e^{-(m/\eta)^2/2} & , m \geq 0, \\ 0 & , m < 0. \end{cases}$$

To estimate η, a histogram (probability) of $\|\Delta f\|$ was computed, and then iterative curve fitting was applied. Under this model, the probability p of noise removal for a particular threshold τ can be calculated by

$$p = \frac{\int_0^\tau Pr_{\|\Delta f\|}(m)dm}{\int_0^\infty Pr_{\|\Delta f\|}(m)dm},$$

and thus $\tau = \sqrt{-2\ln(1-p)}\ \eta$. For $p = 0.999$, $\tau = 3.7\eta$.

Figure 7.9 compares the performance of existing approaches. In (b), we observed that enhancement without any denoising results in distracting background noise. In (c), edges were smeared and broadened by low-pass enhancement. Only in (d), with wavelet shrinkage, enabled were we were to achieve the remarkable result of denoising and contrast enhancement simultaneously.

To demonstrate the denoising process, Figure 7.10 (a) and (b) shows both nonlinear enhancement of wavelet coefficients without and with denoising, respectively, for the original input signal shown in Figure 7.9 (a). Figure 7.10 (c) shows the associated curve-fitting for threshold estimation.

7.6 Two dimensional extension

For image processing applications, the one dimensional structures discussed previously were simply extended to two dimensions. In our investigation, we first adopted the method proposed by Mallat [20], shown in Figure 7.11,

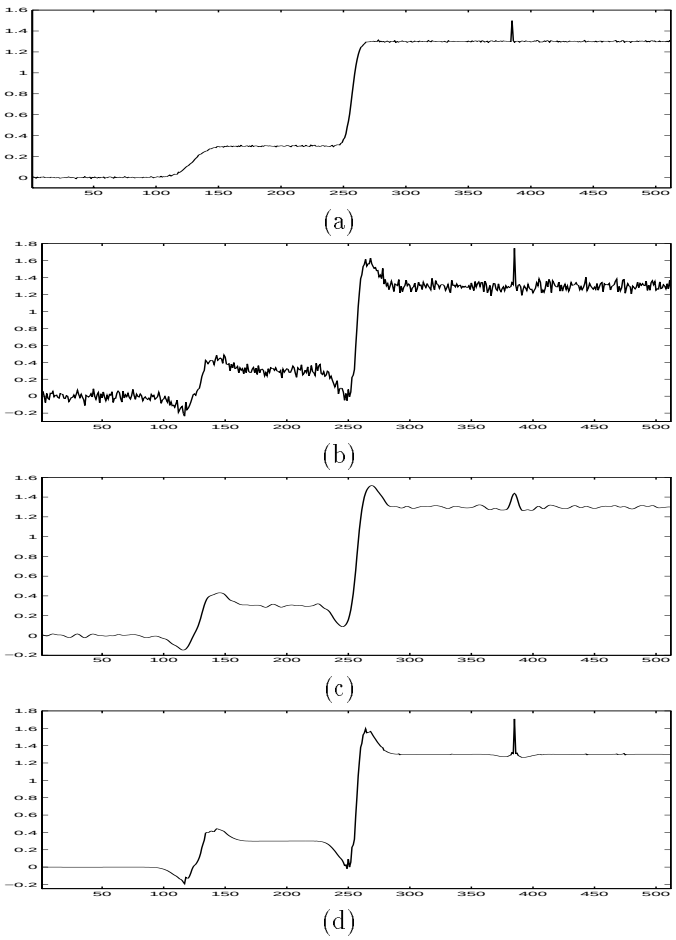

Figure 7.9: (a) Noisy input signal (contaminated by white Gaussian noise). (b) Nonlinear enhancement without denoising, $G_m = 10$, $N = 4$, $t = 0.1$. (c) Nonlinear enhancement of levels 2-3, $G_m = 10$, $t = 0.1$; levels 0-1 zeroed out; (d) Nonlinear enhancement with adaptive wavelet shrinkage denoising, $G_m = 10$, $N = 4$, $t = 0.1$.

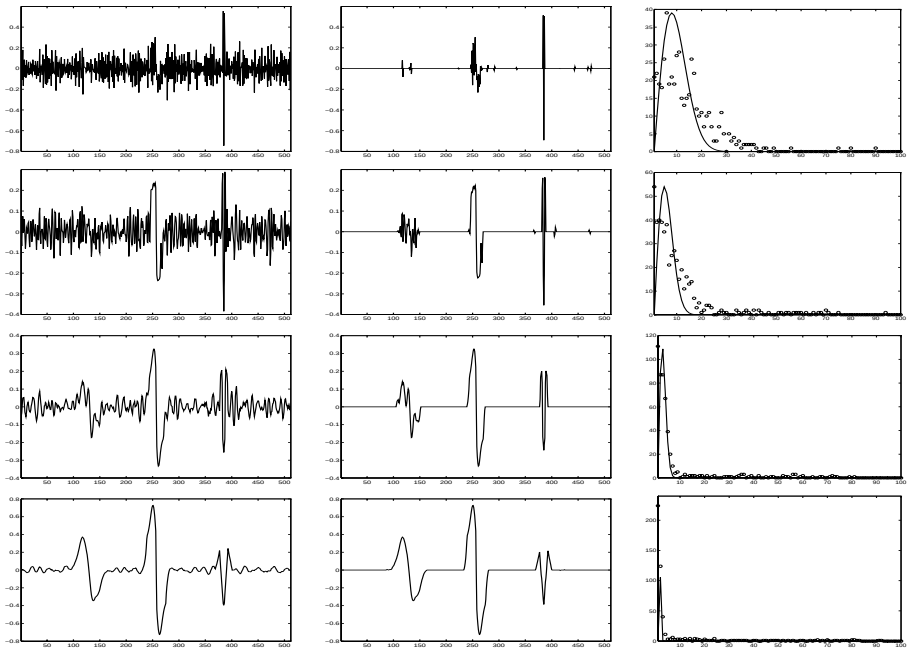

(a) (b) (c)

Figure 7.10: Column (a), Enhanced wavelet coefficients without denoising. Column (b), Enhanced wavelet coefficients with adaptive thresholding $T_n = 4.5\eta$. Column (c), The magnitude distribution and curve-fitting. (Rows 1 through 4 corresponds to levels 1 to 4.)

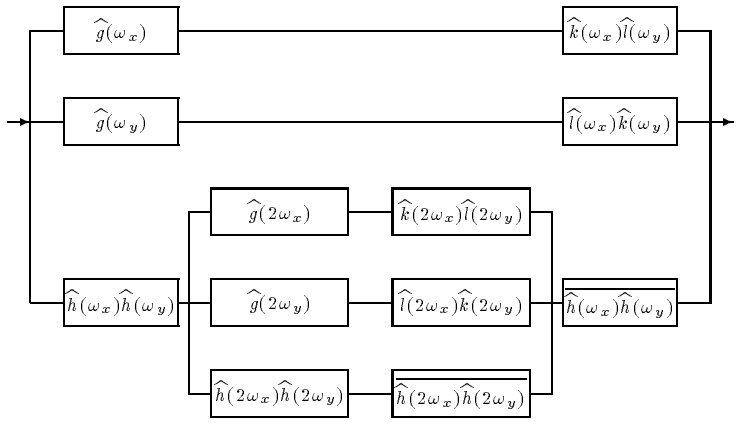

Figure 7.11: Two dimensional dyadic wavelet transform (two levels shown).

where filter $\widehat{l}(\omega) = \left(1 + \left|\widehat{h}(\omega)\right|^2\right)/2$, and $\widehat{h}(\omega)$, $\widehat{k}(\omega)$ and $\widehat{g}(\omega)$ were the same filters constructed for the 1-D case.

However, experimentally we observed that if we simply modified the two oriented wavelet coefficients independently, orientation distortions were introduced. One way to avoid this disastrous artifact is first to apply denoising to the magnitude of gradient coefficients, and then nonlinear enhancement to the sum of the Laplacian coefficients, as shown below in Figure 7.12. For the two oriented gradient coefficients g_x and g_y, the magnitude M and phase P were computed as $M = \sqrt{g_x^2 + g_y^2}$ and $P = \arctan(g_y/g_x)$, respectively. The denoising operation was then applied to M, obtaining M'. The denoised coefficients were then simply restored as $g'_x = M' * \cos(P)$ and $g'_y = M' * \sin(P)$, respectively. For the enhancement operation, notice that the sum of two Laplacian components is *isotropic*. Therefore, we may compute the sum of the two Laplacian components $L = l_x + l_y$ and $F = l_x/L$. A nonlinear enhancement operator was then applied to only L, producing L'. Thus, the restored components were $l'_x = L' * F$ and $l'_y = L' * (1 - F)$.

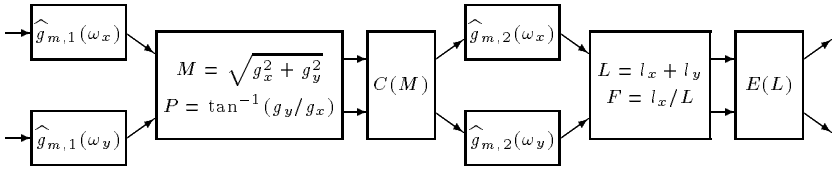

Figure 7.12: Denoising and enhancement for the 2-D case (level one shown).

7.7 Experimental results and comparisons

In this section, we present samples of experimental results and compare them with existing state-of-the-art techniques. Figure 7.13 (a) shows a synthetic image with three circular "bumps" and added white noise. The enhancement results shown in (b) and (c) demonstrate amplification of unwanted noise. Moreover, note that histogram equalization processing alters the object's boundary. However, the result shown in (d) accomplished by dyadic wavelet analysis produced a clearer image without orientation distortion.

Figure 7.14 (a) shows an original dense mammogram image with an obvious mass. The boundary of the mass in the enhanced image is more defined and the penetration of spicules into the mass is well delineated.

To study the efficacy of our algorithm, we blended mathematical phantom features into clinically proved cancer free mammograms. Figures 7.15 (a) and (b) show mathematical phantom features blended into each image M48 and M56 (resulting in Figure 7.16 (a) and Figure 7.17 (a)), respectively.

Figure 7.16 (a) shows a dense mammogram with blended phantom features, and (b) shows an image processed by our nonlinear method. The enhanced image makes more visible the boundary (uncompressed areas) of the breast and its structure. In addition, the phantom features were also well enhanced. Figure 7.17 (a) shows a dense mammogram with blended

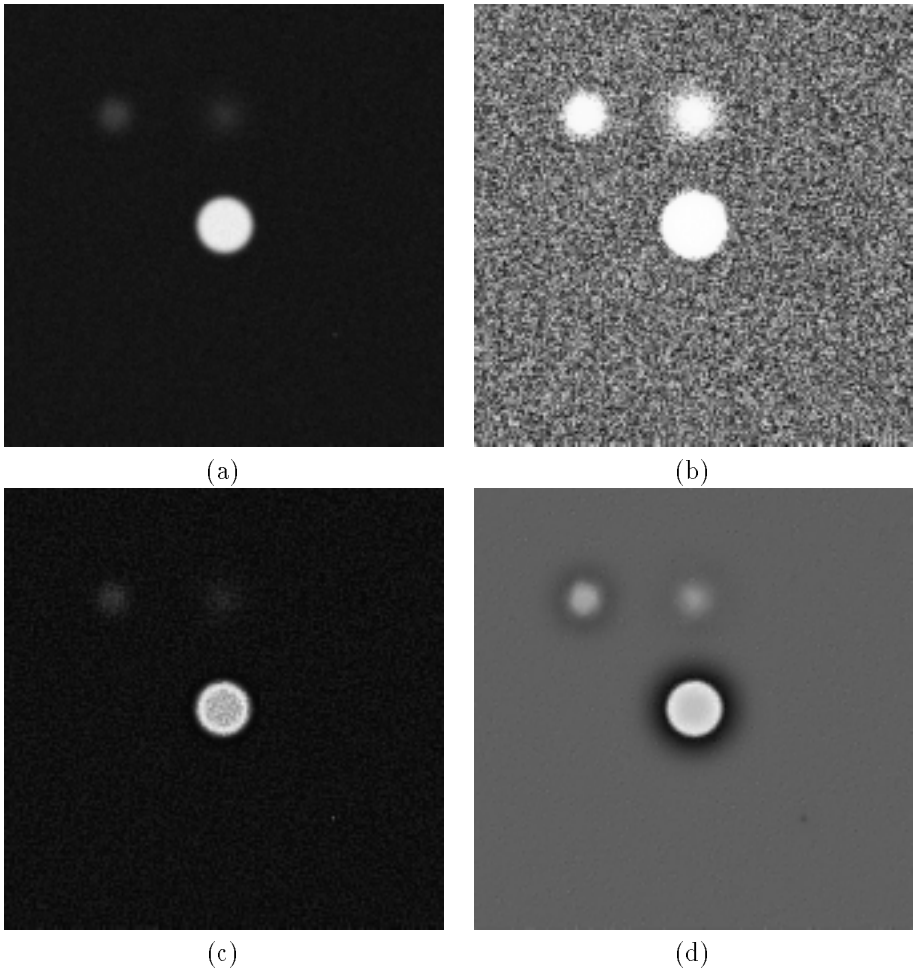

(a) (b)

(c) (d)

Figure 7.13: (a) Noisy image (white Gaussian noise contaminated). (b) Histogram equalized. (c) Nonlinear enhancement by Beghdadi and Negrate's algorithm. (d) Nonlinear enhancement with adaptive wavelet shrinkage denoising, $G_m = 20$, $N = 4$, $t = 0.1$.

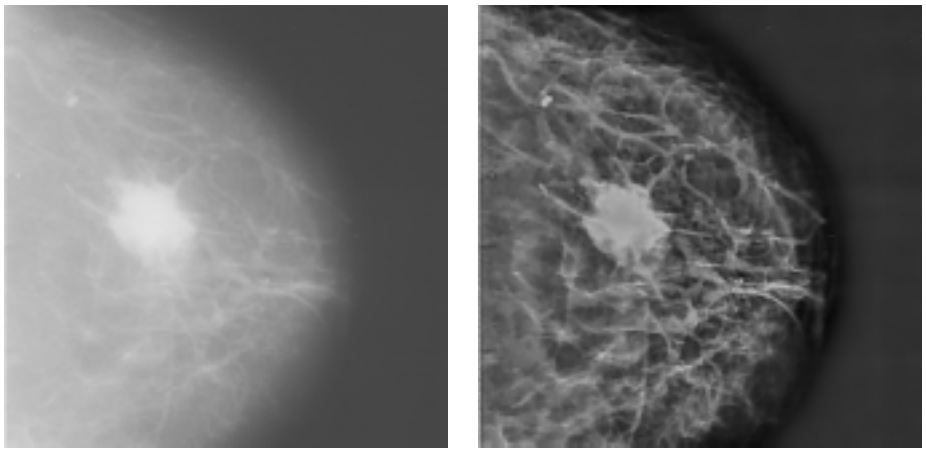

(a) (b)

Figure 7.14: (a) Oringinal mammogram image M73. (b) Nonlinear enhancement with adaptive wavelet shrinkage denoising, $G_m = 20$, $N = 5$, $t = 0.1$.

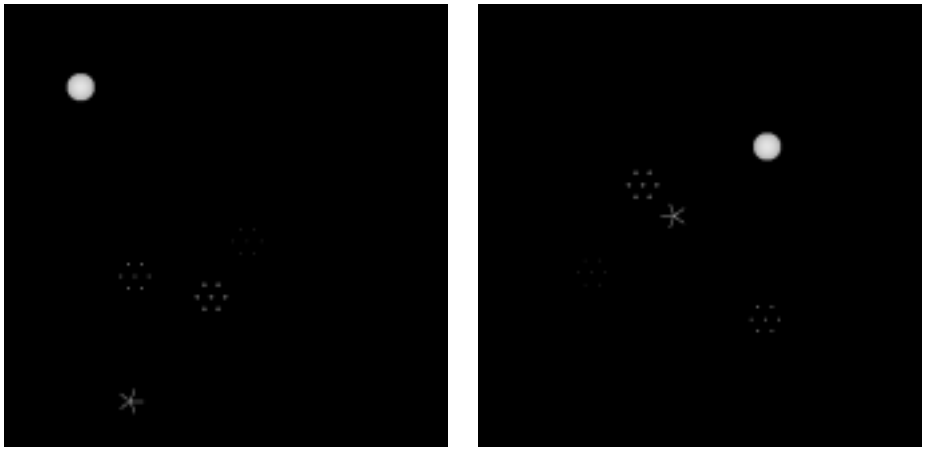

(a) (b)

Figure 7.15: (a) Five phantom features blended into M48. (b) Five phantom features blended into M56.

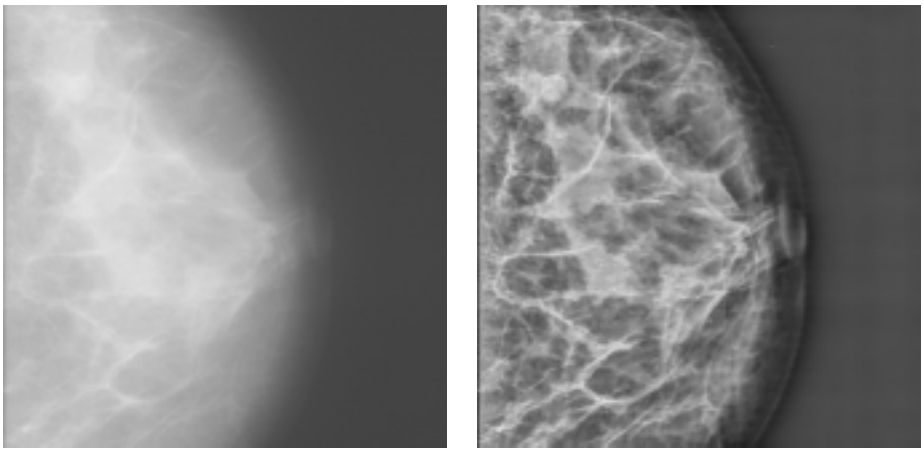

(a) (b)

Figure 7.16: (a) Mammogram image M48 with blended phantom features. (b) Nonlinear enhancement with adaptive wavelet shrinkage denoising, $G_m = 20$, $N = 5$, $t = 0.1$.

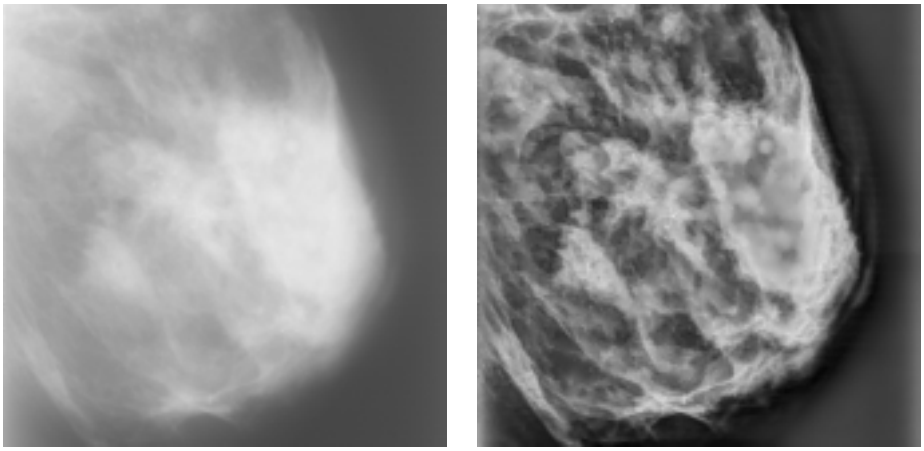

(a) (b)

Figure 7.17: (a) Mammogram image M56 with blended phantom features. (b) Nonlinear enhancement with adaptive wavelet shrinkage denoising, $G_m = 20$, $N = 5$, $t = 0.1$.

phantom features, and (b) shows the associated image enhanced.

7.8 Conclusion

We established connections between dyadic wavelet enhancement algorithms and traditional unsharp masking. We proved that two cases of linear enhancement were mathematically equivalent to traditional unsharp masking with Gaussian low-pass filtering. We designed a methodology for accomplishing nonlinear enhancement with a simple nonlinear function to overcome the wide dynamic range usually required for contrast enhancement of digital radiographs. By careful selection of wavelet filters and enhancement functions, we showed that artifacts could be minimized. An additional advantage of our simple enhancement function is that it includes traditional unsharp masking as a subset.

We then showed how an edge-preserved denoising stage (wavelet shrinkage) can be appropriately incorporated into our contrast enhancement framework, and introduced a method for adaptive threshold estimation. Finally, we showed how denoising and enhancement operations should be carried out for two dimensional images to avoid distortions due to filter orientation.

Our future research plan shall include the systematic study of gain and threshold parameters for nonlinear enhancement. In addition, in the next year we plan to develop localized and complex nonlinear methods to improve the performance of our existing algorithm.

Acknowledgment

This work was sponsored in part by the Whitaker Foundation, and the U.S. Army Medical Research and Development Command, Grant number DAMD17-93-J-3003. The authors wish to thank Doctors Walter Huda, Barbara Steinbach and Janice Honeyman, of the Department of Radiology, Shands Hospital, University of Florida, Gainesville, for their valuable assistance.

References

[1] D. C. Wang, A. H. Vagnucci and C. C. Li. Digital image enhancement: a survey. *Computer Vision, Graphics, and Image Processing*, 24:363-381, 1983.

[2] R. Hummel. Histogram modification techniques. *Computer Graphics and Image Processing*, 4:209-224, 1975.

[3] W. Frei. Image enhancement by histogram hyperbolization. *Computer Graphics and Image Processing*, 6:286-294, 1977.

[4] S. M. Pizer, E. P. Amburn, *et al.* Adaptive histogram equalization and its variations. *Computer Vision, Graphics, and Image Processing*, Vol. 39, 355-368, 1987.

[5] JW Oestmann, R Greene, *et al.* High frequency edge enhancement in the detection of fine pulmonary lines: parity between storage phosphor digital images and conventional chest radiograph. *Invest Radio*, 24:643-646, 1989.

[6] M Prokop, M Galanski, *et al.* Storage of phosphor versus screen-film radiography: effect of varying exposure parameters and unsharp mask filtering on the detectability of cortical bone defects. *Radiology*, 177:109-113.

[7] A. Rosenfeld and A.C. Kak. *digital picture processing. Academic Press, Second edition*, New York, 1982.

[8] L.D. Loo, K. Doi and C.E. Metz. Investigation of basic imaging properties in digital radiograpgy. 4. effect of unsharp masking on the detectability of simple patterns. *Med. Phys.*, 12(2):209-214, 1985.

[9] F. Neycenssac. Contrast enhancement using the Laplacian-of-a-Gaussian filter. *CVGIP: Graphical Models and Image Processing*, 55(6):447-463, 1993.

[10] R. Gordon and R. M. Rangayan. Feature enhancement of film mammograms using fixed and adaptive neighborhood. *Appl. Opt.*, 23:560-564 ,1984.

[11] A. Beghdadi and A. L. Negrate. Contrast enhancement technique based on local detection of edges. *Comput. Vision Graphics Image Process.* 46:162-174, 1989.

[12] A. Laine. Multiscale wavelet representations for mammographic feature analysis. In *Image Enhancement Techniques: Computer Science, National Cancer Institute Breast Imaging Workshop: State-of-the-Art and New Technologies*, Bethesda, MD, 1991.

[13] A. Laine, S. Song. Multiscale wavelet representations for mammographic feature analysis. In *Proceedings of SPIE: Conference on Mathematical Methods in Medical Imaging*, San Diego, CA, 1992.

[14] A. Laine, S. Song. Wavelet processing techniques for digital mammography. In *Proceedings of SPIE: Conference on Visualization in Biomedical Computing,* Chapel Hill, NC, 1992.

[15] A. Laine, S. Song, J. Fan. Adaptive Multiscale Processing for Contrast Enhancement. In *Proceedings of SPIE: Conference on Biomedical Imaging and Biomedical Visualization,* San Jose, CA, 1993.

[16] B. D. Jawerth, M. L. Hilton and T. L. Huntsberger. Local enhancement of compressed images. *J. Mathematical Imaging and Vision*, 3:39–49, 1993.

[17] A. Laine, S. Schuler, J. Fan, W. Huda. Mammographic feature enhancement by multiscale analysis. *IEEE Trans. on Medical Imaging*, 13(4):725–740, 1994.

[18] J. Lu and D.M. Healy Jr. Contrast enhancement of medical images using multiscale edge representation. In *Proceedings of SPIE: Wavelet applications,* Orlando, FL, 1994.

[19] S.Mallat. A theory for multiresolution signal decomposition : the wavelet representation. *IEEE Trans. Pattern Anal. Machine Intell.*, 11:674–693, 1989.

[20] S.Mallat and Sifen Zhong. Characterization of signals from multiscale edges. *IEEE Trans. Pattern Anal. Machine Intell.*, 14:710–732, 1992.

[21] P. Perona nad J. Malik. Scale-space and edge detection using anisotropic diffusion. *IEEE Trans. Pattern Anal. Machine Intell.*, 12:629-639, 1990.

[22] S.Mallat and W. L. Hwang. Sigularity detection and processing with wavelets. *IEEE Trans. Inform. Theory*, 38(2):617–643, 1992.

[23] D. L. Donoho. Nonlinear wavelet methods for recovery of signals, densities, and spectra from indirect and noisy data. *Proc. Symposia Applied Math.* , 00:173–205, 1993

[24] H. Voorhees and T. Poggio. Detecting textons and texture boundaries in natural images. *Proc. First International Conference on Computer Vision*, pages 250–258, 1987.

Index